HHS Public Access

Author manuscript

Nature. Author manuscript; available in PMC 2021 January 11.

Published in final edited form as:

Nature. 2020 April ; 580(7802): 239–244. doi:10.1038/s41586-020-2158-3.

Local and global consequences of reward-evoked striatal dopamine release

Nan Li[1], **Alan Jasanoff**[1,2,3]

[1]Department of Biological Engineering, Massachusetts Institute of Technology, 77 Massachusetts Ave. Rm. 16-561, Cambridge, MA 02139

[2]Department of Brain & Cognitive Sciences, Massachusetts Institute of Technology, 77 Massachusetts Ave. Rm. 16-561, Cambridge, MA 02139

[3]Department of Nuclear Science & Engineering, Massachusetts Institute of Technology, 77 Massachusetts Ave. Rm. 16-561, Cambridge, MA 02139

Abstract

The neurotransmitter dopamine is required for the reinforcement of actions by rewarding stimuli[1]. Neuroscientists have tried to define dopamine's functions in concise conceptual terms[2], but the practical significance of dopamine release depends on its diverse brain-wide consequences. Although the molecular and cellular effects of dopaminergic signaling have been extensively studied[3], its impact on larger-scale neural activity profiles is less understood. Here we combine dynamic dopamine-sensitive molecular imaging[4] and functional magnetic resonance imaging (fMRI) to determine how striatal dopamine release shapes local and global responses to rewarding stimulation in the rodent brain. We find that dopamine consistently alters the duration but not the magnitude of stimulus responses across much of striatum, via quantifiable postsynaptic effects that vary across subregions. Striatal dopamine release also potentiates a network of distal responses we delineate using neurochemically-dependent functional connectivity analyses. Hot spots of dopaminergic drive notably include cortical regions associated with both limbic and motor function. Our results thus reveal distinct neuromodulatory actions of striatal dopamine that extend well beyond its sites of peak release, and that result in enhanced activation of remote neural populations necessary for performance of motivated actions. Our findings also suggest brain-wide biomarkers of dopaminergic function and could provide a basis for improved interpretation of neuroimaging results relevant to learning and addiction.

Address correspondence to AJ, phone: 617-452-2538, jasanoff@mit.edu.

Author Contributions N.L. and A.J. designed the research, interpreted the results, and wrote the paper. N.L. conducted all of the experiments and analyzed the data.

Online content Methods and Extended Data display items are available in the online version of the paper.

Author Information Reprints and permissions information is available at www.nature.com/reprints. The authors declare no competing interests. Readers are welcome to comment on the online version of the paper. Correspondence and requests for materials should be addressed to A.J. (jasanoff@mit.edu).

Data availability Raw datasets generated for the current study are available from the corresponding author on reasonable request.

To permit combined fMRI and molecular neuroimaging of dopamine during phasic reward signaling, rats were unilaterally implanted with cannulae targeting ventral striatum and electrodes targeting the lateral hypothalamus (LH) (Fig. 1a), a structure containing neurochemically diverse axonal fibers whose stimulation provides robust behavioral reinforcement[5]. Animals were tested for self-stimulation behavior (Extended Data Fig. 1) and then lightly sedated and placed in a 9.4 T magnetic resonance imaging (MRI) scanner. Scanning was performed during and after pre-infusion of the dopamine-sensitive protein-based MRI contrast agent BM3h-9D7 (9D7)[6] via the cannulae, followed by continued infusion together with LH stimulation matching conditions used in the behavioral tests. A multi-gradient echo MRI pulse sequence was used for readout[7], providing simultaneous indication of T_1 effects arising from the dopamine sensor and blood oxygen level-dependent (BOLD) contrast reflective of neural population activity (Fig. 1b and Extended Data Fig. 2a).

Selectivity of sensor-mediated responses was verified by comparing T_1-weighted signal in the presence of 9D7 with equivalent data from separate animals injected with a control contrast agent, BM3h-WT (WT), which lacks dopamine sensitivity but otherwise displays similar characteristics to 9D7 and differs by only four point mutations (Fig. 1c)[8]. Although hemodynamic responses are largely suppressed in the presence of either agent (Extended Data Fig. 2b,c), comparison of 9D7 and WT-mediated MRI signals also enables identification of slow residual hemodynamic signals, of opposite polarity to the dopamine response, that are present in the T_1-weighted time courses (Fig. 1d). These residual signals could be removed by voxel-level baseline correction based either on the mean WT response or the echo time-dependent component of the 9D7 response (Extended Data Fig. 3).

A map of peak stimulus-dependent dopamine release was determined for a 9D7-infused region encompassing the nucleus accumbens (NAc), medial caudate-putamen (mCPu), olfactory tubercle (Tu), and lateral septal area (LS) (Fig. 2a). Voxel-level dopamine concentrations were derived from the MRI data from five rats, using a signal modeling approach that is robust to differences in the concentration of contrast agent among voxels (see Methods and Extended Data Fig. 4a)[4]. The absence of dopamine-independent signals was confirmed in data obtained using the WT control (Extended Data Fig. 4b,c). Statistical analysis (Extended Data Fig. 4d,e) indicates that the 9D7-dependent profile contains clear spatial features such as a pronounced peak of dopamine release in NAc. A corresponding striatal map of BOLD fMRI responses to LH stimulation was also obtained (Fig. 2b)[9,10]; a separate group of five uninjected animals was used for this, in order to avoid the attenuating effects of contrast agent on hemodynamic signals in the areas of infusion (Fig. 1 and Extended Data Fig. 2).

Reward-related striatal BOLD responses have previously been thought to represent dopaminergic activity[11,12], but comparison of BOLD and dopamine data in our experiments reveals notable differences. Although widespread signals are apparent in both imaging modalities, the ratio of the two signal magnitudes varies substantially over the areas we investigated (Fig. 2c). Average dopamine amplitudes are about twice as high in NAc and mCPu, compared with Tu and LS, whereas BOLD responses are more homogeneous,

varying by less than 15% of the mean amplitude among striatal regions of interest (ROIs) (Fig. 2d–e).

Dopamine and hemodynamic fMRI responses to rewarding stimulation differ temporally and as a function of stimulus strength as well (Fig. 2f–g). Amperometry recordings show that dopamine release and removal track stimulation blocks with a full width at half maximum (FWHM) of about 20 s (Extended Data Fig. 5a). Dopamine-dependent MRI responses exhibit broadening due to the influence of sensor binding kinetics (Extended Data Fig. 5b,c), but occur on a similar time scale and track predicted total dopamine levels with high fidelity. The FWHM of the dopamine responses averages 40 ± 6 s over the region where peak responses were observed; meanwhile, the mean response amplitude in this area rises approximately linearly with stimulation frequency (Fig. 2h). In contrast, the corresponding BOLD response to stimulation extends for about 200 s following stimulus offset, particularly for 120–200 Hz frequencies; the FWHM reaches 84 ± 8 s, significantly longer than the corresponding dopamine response (*t*-test $p < 0.0001$, $n = 5$). The amplitude of BOLD responses also saturates with increasing stimulus strength. Relative to responses at 120 Hz LH stimulation, mean dopamine release amplitudes at 200 Hz are 50% higher (difference significant with *t*-test $p = 0.03$, $n = 5$), whereas BOLD responses are virtually the same at 120 and 200 Hz (*t*-test $p = 0.58$, $n = 5$).

The discrepancies between striatal dopamine and BOLD signals could arise from non-dopaminergic activity[13] or from postsynaptic contributions of dopamine to the BOLD responses. To evaluate these possibilities, we performed a second set of hemodynamic fMRI experiments before and after systemic injection of a cocktail including the dopamine D1 and D2 receptor antagonists SCH 23390 and eticlopride (Fig. 3a). Treatment with this cocktail improved the voxel-level correlation between mean dopamine and BOLD responses to rewarding stimulation throughout much of the medial striatum (Fig. 3b). 77% of voxels show increased correlation between dopamine and BOLD signals after D1/D2 receptor inhibition, with 10% of voxels showing significant improvement ($\Delta Z > 2.0$) at an individual level. This suggests that dopamine's postsynaptic effects contribute substantially to differences between response profiles presented in Fig. 2.

Inhibition of dopamine receptors also increased the topographic similarity of the dopamine and BOLD amplitude maps, as reflected by a reduction in the deviation from direct proportionality of dopamine and BOLD response magnitudes across all voxels in the field of view (Extended Data Fig. 6a). The root mean squared deviation from proportionality decreased by 25% after D1/D2 blockade, a significant change with *F*-test $p = 0.0019$; this coincided with an increase in correlation coefficient between dopamine and BOLD from –0.16 (significant with $p = 0.001$) before D1/D2 inhibition to 0.01 ($p = 0.8$) after inhibition. Significant improvements by 23–44% in the proportionality between dopamine and BOLD were also apparent within striatal subregions NAc, mCPu, and LS (*F*-tests $p \leq 0.005$) (Fig. 3c).

These effects arise in part from dopamine receptor-dependent changes in BOLD fMRI response amplitudes. In the presence of blockers, the distribution of voxel-wise BOLD amplitudes is significantly lower in mCPu, LS, and Tu (19–33% changes, paired *t*-test $p \leq$

0.05), but not in NAc (8% change, n.s. with $p = 0.13$) (Fig. 3d). More striking, however, is the effect of dopamine receptor inhibition on fMRI time courses in the striatum. All ROIs experience substantial decreases in response duration (Fig. 3e; individual FWHM decreases all significant with *t*-test $p \leq 0.04$), resulting in values comparable to dopamine release time courses themselves (Fig. 2g). In contrast, treatment with dopamine blockers barely changes the spatiotemporal properties of dopamine release (Extended Data Fig. 6b–d), indicating that feedback onto dopamine release itself does not play a substantial role in the inhibitor-mediated effects.

Taken together, these results indicate that postsynaptic effects of dopamine contribute significantly to the discrepancy between rewarding stimulus-evoked BOLD fMRI and dopamine signals in striatal subregions, and that reward-evoked striatal fMRI signals cannot be explained in terms of input alone[14]. By comparing D1/D2 blocker-dependent changes in the BOLD signal with the dopamine data of Fig. 1 we determined a spatiotemporal impulse response function that describes the net effects of dopamine at each voxel (Fig. 3f) and in each striatal ROI (Fig. 3g). This analysis suggests that the primary effect of dopamine is to modulate the duration of fMRI-detectable responses to stimulation. Dopamine's effects on the magnitudes of brain activation appear to be subtler and more variable across striatal subregions, perhaps because of regional differences in receptor densities and occupancies[15].

We hypothesized that long-range consequences of striatal dopamine release could be discovered by identifying brain-wide fMRI signals correlated with the dopamine response characteristics. BOLD fMRI data obtained from rats untreated with contrast agent show that rewarding stimulation evokes activation in a broad range of structures throughout the rostral half of the brain (bregma –1.5 mm to +3.5 mm) (Fig. 4a). To locate responses that might be particularly closely related to striatal dopamine, we first computed the average time course of each voxel's fMRI signal at each stimulus strength. We then applied voxel-wise multiple regression analysis using the mean striatal dopamine time courses at each stimulus strength (Fig. 2f) and the global BOLD signal as regressors; the fraction of preferentially dopamine-tracking variance was quantified at each position in the brain (Fig. 4a, middle row). At an ROI level (Fig. 4b and Extended Data Fig. 7), this analysis revealed particularly strong dopamine tracking behavior by BOLD signals in CPu, motor cortex (MCx), insular cortex (ICx), secondary somatosensory cortex (S2), and LH (*Z*-test $p \leq 0.05$, $n = 5$; all ROIs ipsilateral to stimulation). Lesser or negligible dopamine tracking was observed in NAc, Tu, LS, cingulate cortex (CCx), and ventral pallidum (VP) (*Z*-test $p \geq 0.05$, $n = 5$), despite the fact that rewarding stimuli evoke comparable BOLD amplitudes in these regions.

Strikingly, most regions with strongly dopamine-tracking fMRI signals also display high sensitivity to D1/D2 blockade during stimulation (Fig. 4a, bottom row), providing additional support for a connection between these regions and dopaminergic function. Strong and consistent blocker-dependent suppression of BOLD signals is observed in CPu, MCx, ICx, and S2 (before *vs.* after *t*-test $p \leq 0.0001$) (Fig. 4b). Weaker D1/D2 blocker sensitivity is observed in Tu ($p = 0.047$), which does not exhibit strong dopamine tracking in the regression analysis, and negligible effects ($p \geq 0.09$) are observed in LS, CCx, VP, NAc, and LH. A similar profile of fMRI signal changes was observed upon infusion of D1 and D2 inhibitors into cerebrospinal fluid, suggesting that the blocker-dependent difference signals

do not reflect systemic physiological changes (Extended Data Fig. 8). The D1/D2 blocker and dopamine tracking effects in MCx, ICx, and S2 seem surprising, given that these cortical regions receive relatively sparse presynaptic dopamine input[16,17]. This raises the possibility that striatal dopamine indirectly modulates reward-evoked activation in the cortex, and could help explain evidence linking MCx and ICx in particular to reward-related functions[18,19,20].

We reasoned that if striatal dopamine release were causally related to distal BOLD responses, then variation of striatal dopamine release profiles across animals—due to factors such as electrode placement or individual differences—would correlate with variations in BOLD signals at the distal sites. We tested this idea by using the mean BOLD responses at each ROI as components of a regression analysis of dopamine responses measured simultaneously within the same animals. Fig. 4c maps the extent to which striatal dopamine signals track BOLD responses in CPu, MCx, ICx, S2, and LH across five animals; Fig. 4d diagrams corresponding results averaged over striatal ROIs. These data indicate that MCx, ICx, and S2 signals do in fact correspond closely to striatal dopamine (Fig. 4d), especially in NAc and mCPu (regression coefficients ≥ 0.12, *t*-test $p \leq 0.045$). In contrast, BOLD signals in LH and in lateral CPu (defined to avoid overlap with contrast agent-infused mCPu regions) do not correspond to dopamine measurements from striatal ROIs. Notably, this correspondence between striatal dopamine release and distal BOLD signals observed across individual animals is sharply reduced in the presence of D1/D2 blockers (Extended Data Fig. 9), further implying a causal role for dopamine in the observed effects.

As an additional test of the relationship between striatal dopamine and cortical BOLD responses, we infused SCH 23390 and eticlopride locally into ventral striatum and examined effects on LH stimulus-induced activation. Like the global inhibition experiment in Fig. 4a, this experiment also reveals substantial peaks of difference signal in cortical regions, confirming that striatal dopaminergic signaling contributes to modulation of distal BOLD signals (Fig. 4e and Extended Data Fig. 10a). Peak responses in MCx, ICx, and S2 were 0.6–0.9% lower on average in the presence *vs.* absence of striatal D1/D2 inhibition; these decreases were significant with paired *t*-test $p \leq 0.05$ (Fig. 4f). Similar results were obtained using striatal infusions that contained the α2 adrenergic inhibitor yohimbine in addition to the D1/D2 blockers (Extended Data Fig. 10b), supporting specificity of the findings to dopaminergic function and suggesting that α2 agonism by the medotomidine sedative used in these experiments does not alter the outcome.

A straightforward interpretation of these results is that feedforward effects of phasic dopamine release in NAc and mCPu causally modulate fMRI responses in the distal cortical regions[21], probably via polysynaptic mechanisms. Meanwhile, the fact that LH and CPu show strong dopamine tracking in Fig. 4b most likely indicates that these regions receive stimulus-dependent input that temporally parallels but does not depend on ventral striatal dopamine release. The fact that LH is not sensitive to systemic D1/D2 inhibition further suggests that its activation is mediated by nondopaminergic mechanisms[22], consistent with relatively weak hypothalamic responses previously reported upon postsynaptic stimulation of D1- and D2-expressing striatal neurons[23]. These findings relate specifically to the consequences of striatal dopamine release but do not rule out additional roles for non-striatal dopamine or non-dopaminergic mechanisms.

Considered together, our results are notable in several key respects. First, they explicitly link striatal dopamine release to a broad constellation of brain responses which could be mechanistically important for carrying out reward-related behaviors. Topographic aspects of these relationships could be characterized because of our specialized imaging approach, and functional connectivity results were particularly strengthened by our ability to map striatal dopamine and global BOLD responses simultaneously within individual animals. Functional connectivity between striatal dopamine domains and diverse brain regions including MCx and ICx suggests a basis for dopamine's multifaceted contributions to motivated action. Second, our results show how dopamine modulates neural response profiles in ways that go beyond simple excitation or inhibition[24], contrasting with previous fMRI-based reports that link optogenetic stimulation of dopaminergic neurons primarily to increases in postsynaptic activity[25,26]. The dopamine-dependent enhancement of striatal response durations we observe could reflect the action of dopaminergic signaling cascades involved in plasticity and learning[27,28,29]. And third, our findings could broadly help explain other neuroimaging results related to dopamine or reward. For instance, our dissociation of dopamine and fMRI signals in ventral striatum could account for previously reported deviations of striatal BOLD responses from predictions of temporal difference learning theory in people[30]. Conversely, the correlates of striatal dopamine release we have identified could provide new biomarkers for assessing dopaminergic function in human and animal brains.

Extended Data

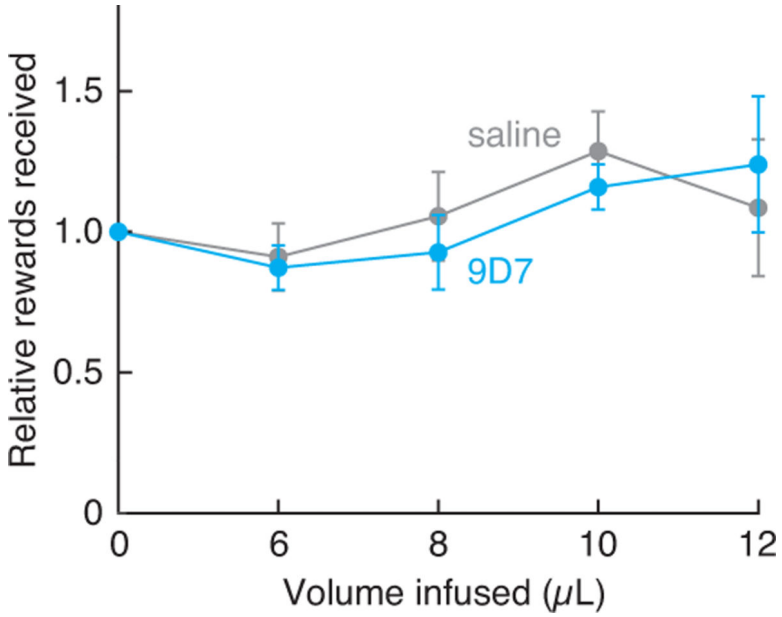

Extended Data Fig. 1 |. Intracranial self-stimulation in the presence and absence of 9D7. Behaviorally shaped rats implanted with unilateral cannulae targeting ventral striatum performed intracranial self-stimulation during continuous injection of 500 μM of the dopamine sensor 9D7 (blue) or saline vehicle (gray), under infusion conditions used for imaging experiments. The number of rewards received per trial is graphed, relative to

rewards received prior to infusion, showing no significant difference between infusion of 9D7 *vs.* saline. Error bars denote SEM of data from $n = 5$ animals each.

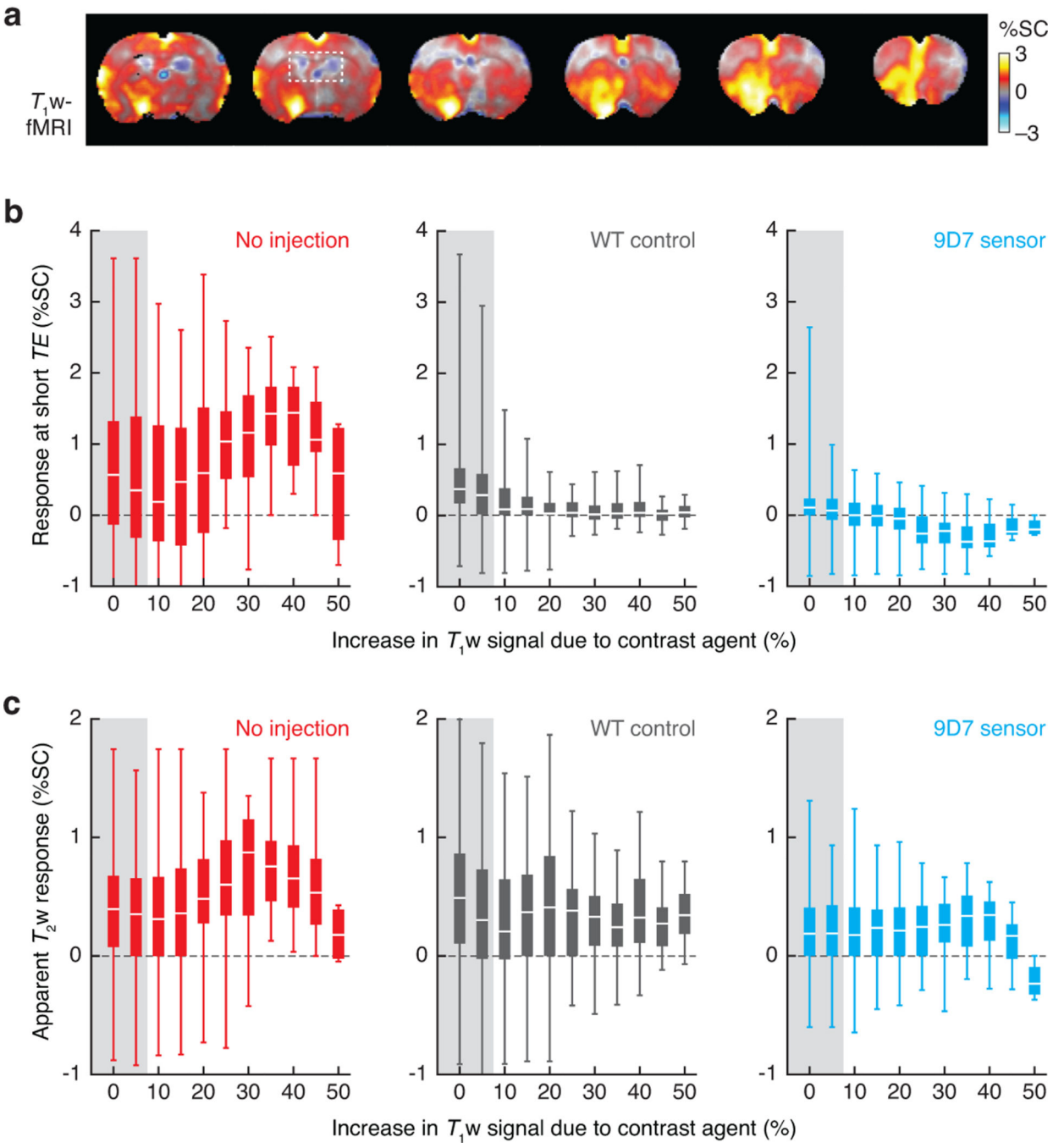

Extended Data Fig. 2 |. Suppression of hemodynamic signals by contrast agents infused into ventral striatum.

a, T_1-weighted fMRI data from uninjected rats. Mean T_1-weighted responses to LH stimulation from five animals that were not injected with MRI contrast agents, measured under conditions identical to those used for the injected animals in Figure 1b. Negative hemodynamic signals in the ventricles are apparent (dotted box). **b,** Striatal voxels were

scored based on the T_1-weighted (T_1w) signal change they experienced following 50 min of contrast agent infusion (9D7 dopamine sensor or WT control protein). Uninjected animals were given a pseudo score based on the signal change experienced by spatially equivalent voxels in animals injected with 9D7. Box plots show LH stimulus-evoked T_1-weighted responses over all voxels as a function of the injection score, in 5% bins, for uninjected animals (left), animals that received infusion of WT protein (middle), and animals that received 9D7 (right). Gray shading indicates bins excluded from molecular imaging analysis due to incomplete suppression of hemodynamic responses. **c,** Equivalent graphs showing variation of T_2-weighted signal obtained using multiecho analysis, as a function of injected contrast agent dose for injected animals or pseudo dose for uninfused animals. All box plots indicate median (white line), first and third quartiles (box), and full data ranges (whiskers) over voxels in each bin. Individual voxel intensities are means over five animals in each condition.

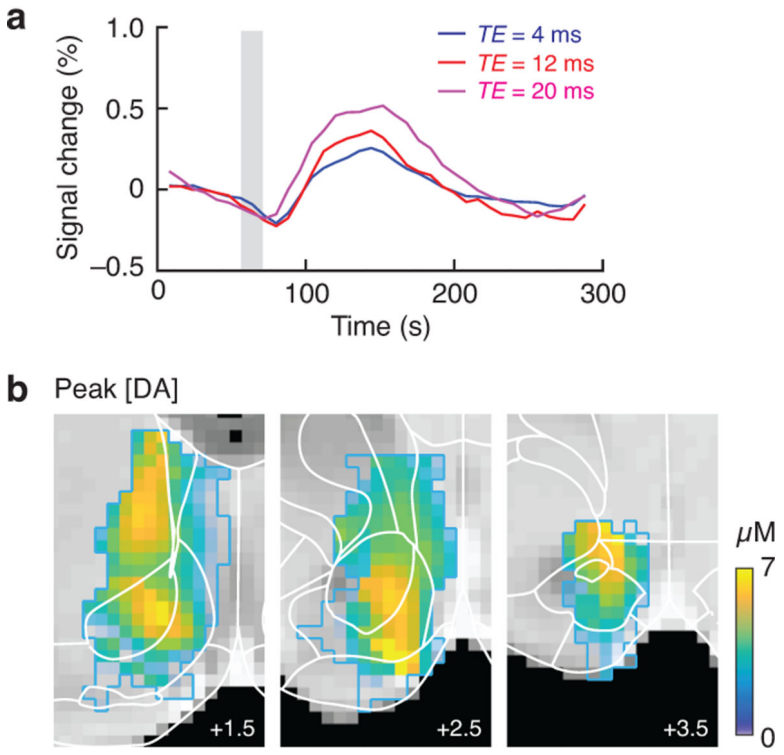

Extended Data Fig. 3 |. Baseline correction of dopamine fMRI data using T_2^*-dependent signals. **a,** Echo time dependence of the slow component of the fMRI signal recorded in the presence of the 9D7 dopamine sensor in ventral striatum. Variation of the slow positive signal with *TE* provides a basis for extracting the baseline time course using the ME-ICA approach. Error margins omitted for graphical clarity. **b,** Quantitative maps of dopamine release formed following baseline correction using the ME-ICA signal. Features correspond closely to the maps in Fig. 2a, which were corrected using a baseline derived from the control WT T_1w fMRI data, indicating that the choice of baseline correction method makes little difference to the outcome.

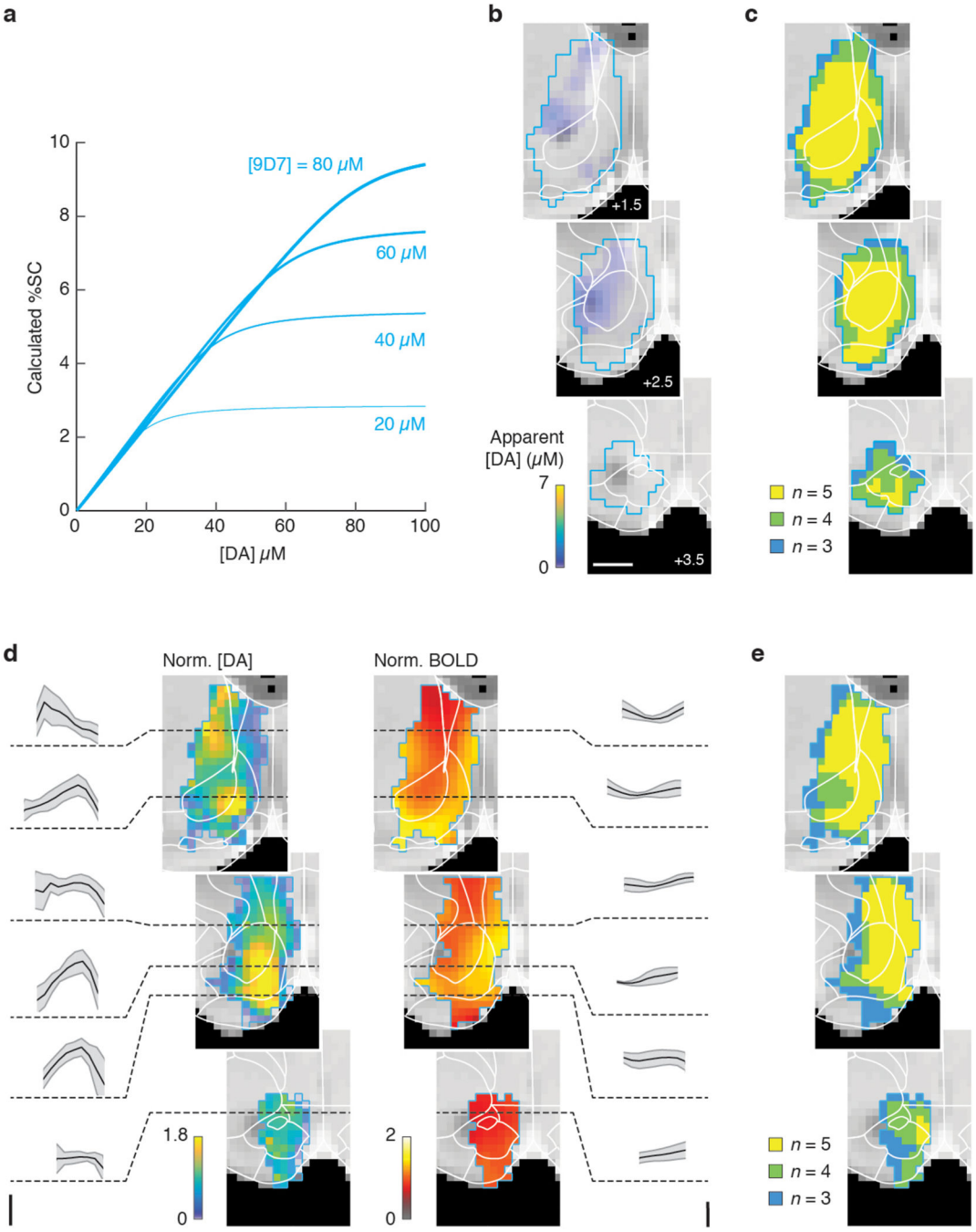

Extended Data Fig. 4 |. Quantification of dopamine concentrations.

a, MRI percent signal changes (%SC) as a function of dopamine concentration ([DA]) were estimated with respect to [DA] = 0 μM from the *in vitro* relaxivity of 9D7 and experimental parameters used in the imaging. **b,** To verify the absence of baseline contributions to dopamine maps obtained with 9D7, mock dopamine imaging was performed using the WT control contrast agent. LH stimulus-induced signal changes were observed in animals injected with the dopamine-insensitive contrast agent WT, and mock dopamine maps were computed as described for molecular imaging experiments using the 9D7 sensor. Scale bar =

1 mm. **c,** Number of animals contributing to data from each voxel in **b**. The results show that minimal dopamine concentrations were observed, indicating effective suppression of background or nonspecific signals to the T_1-weighted data. **c,** Robustness of spatial features in dopamine and BOLD fMRI response maps was verifed by examining average data across animals. Dopamine (DA) release or BOLD fMRI amplitudes from each individual animal contributing to Fig. 2a,b were normalized to the mean response level and standard errors were computed to determine error margins shown in gray shading in the cross sections shown at left (for dopamine) and right (for BOLD). These data indicate that the locations of peak dopamine responses in ventromedial striatum are conserved among animals, while the BOLD responses are relatively uniform across the FOV. Scale bars correspond to 3 μM DA (left) and 1% BOLD signal modulation (right), before normalization. **d,** Number of animals contributing to each voxel of the dopamine data averages in **c**, as well as Fig. 2 in the main text.

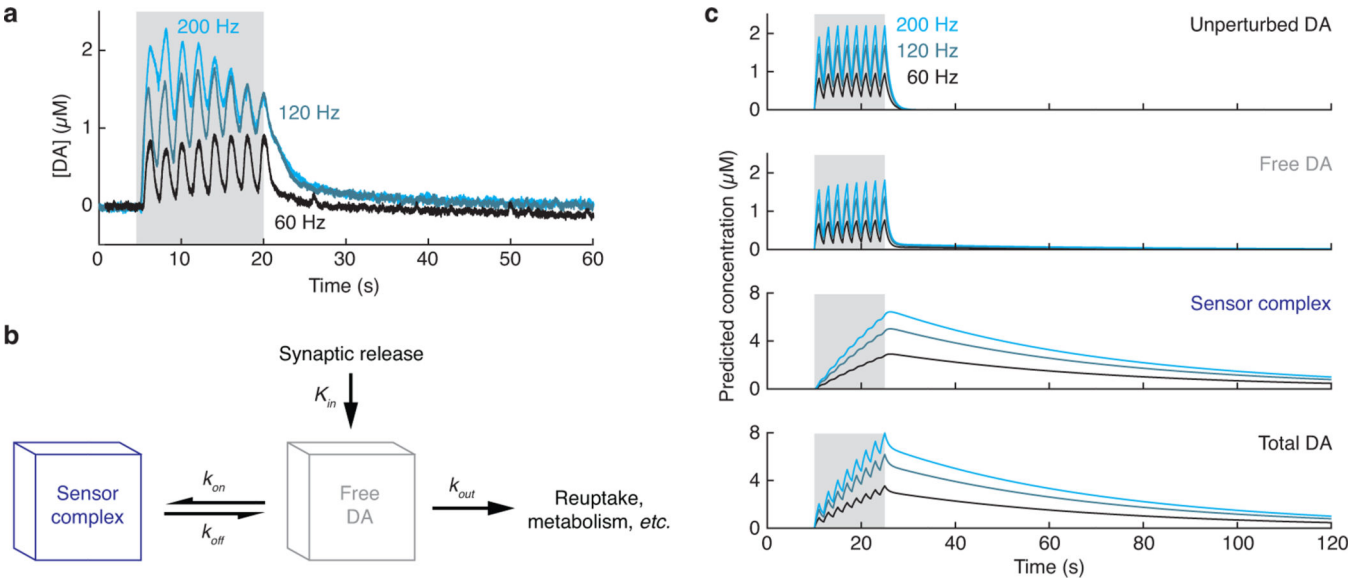

Extended Data Fig. 5 |. Imaging-independent estimation of dopamine release dynamics.
a, Amperometric recording was used to measure dopamine release elicited by LH stimulation. LH stimulation at 60, 120, and 200 Hz frequencies was performed in medetomidine-sedated rats prepared as for functional imaging experiments. Amperometric recordings of a representative rat were obtained using carbon fibers calibrated after *in vivo* recording to obtain absolute measurements of dopamine (DA) concentration. **b,** Diagram of a kinetic model that accounts for introduction of dopamine by synaptic release at the fixed rate K_{in} during stimulation, interconversion of free and 9D7-bound dopamine with rate constants k_{on} and k_{off}, and removal of free dopamine with the rate constant k_{out}. **c,** Simulations were performed using parameters chosen to emulate the amperometry data of Extended Data Fig. 8 in the absence of 9D7, with K_{in} = 1.3, 2.3, and 3 μM/s corresponding to the three stimulus intensities of 60, 120, and 200 Hz, respectively, and a k_{out} value of 1 s^{-1}. Values of k_{on} (0.013 $\mu M^{-1}s^{-1}$) and k_{off} (0.03 s^{-1}) were derived from stopped flow binding data and empirical estimates of dopamine removal rate reported in reference 4. The top trace shows simulated free dopamine concentration in the absence of 9D7 (unperturbed

DA), while the second trace from the top shows simulated free dopamine in the presence of 40 μM 9D7, revealing a modest buffering effect. The bottom two traces depict the simulated sensor complex concentration in the presence of 40 μM 9D7, as well as the total dopamine concentration under these conditions. These results reveal the expected broadening of total dopamine kinetics in the presence of the 9D7 sensor, but also show that the sensor complex concentration closely tracks total dopamine levels in the system.

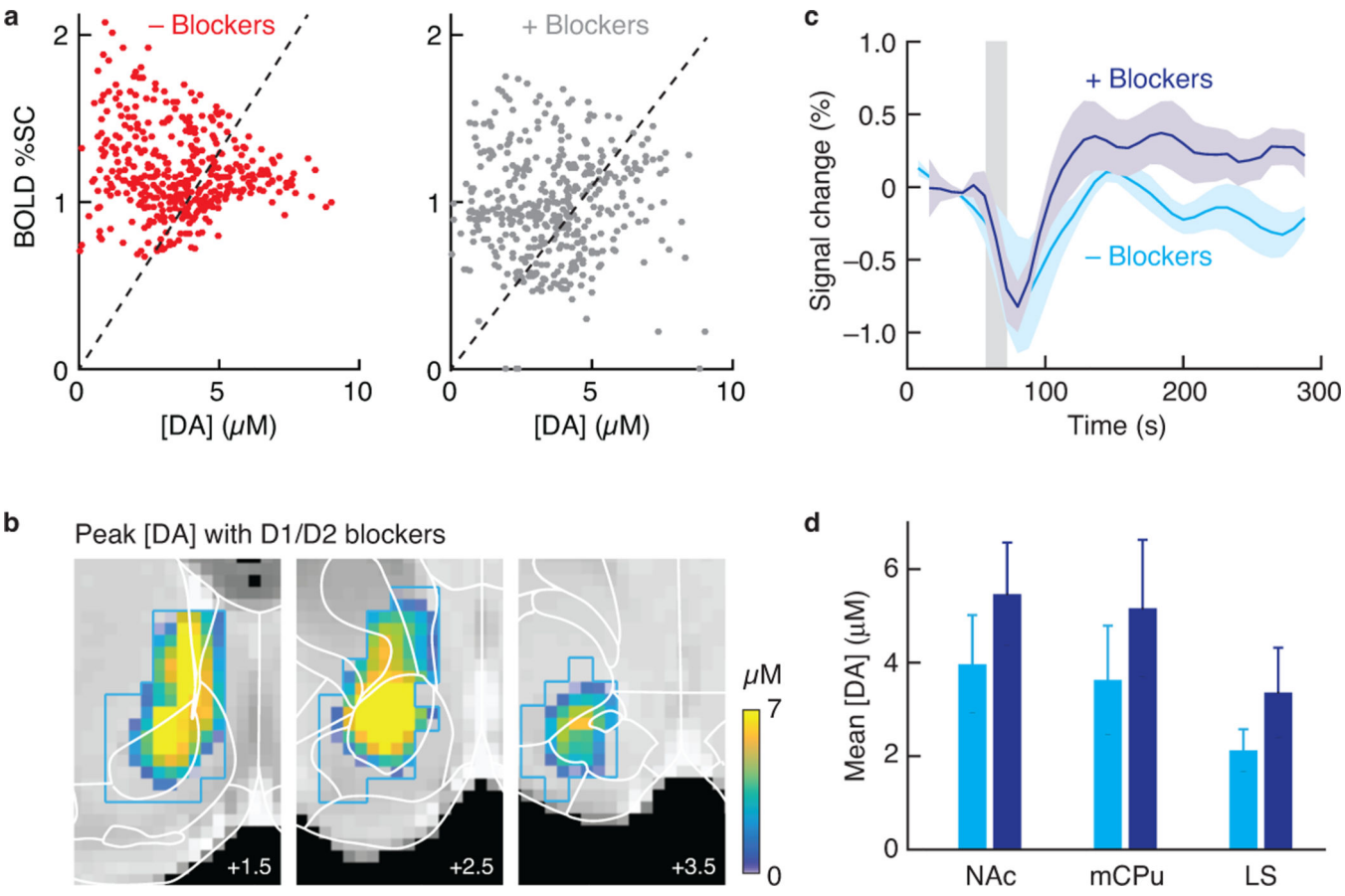

Extended Data Fig. 6 |. Additional effects of dopamine receptor inhibition.

a, Scatter plots display the effects of dopamine inhibitors on the correspondence of mean dopamine concentration ([DA]) and BOLD amplitudes (%SC) evoked by LH stimulation. Each dot denotes one voxel in the absence of dopamine receptor blockers (left), or in the presence of SCH 23390 and eticlopride (right). Dashed lines indicate best fit line of proportionality between the two measures. The addition of D1 and D2 receptor blockers significantly improved the correspondence (*F*-test $p = 0.0019$). **b,** Dopamine inhibition exerts negligible effect on dopamine release *per se*. 9D7 sensor was infused into ventral striatum as for experiments in Figs. 1 and 2, and multigradient imaging we performed to acquire fMRI data in the presence of systemic SCH 23390 and eticlopride treatment. Maps of peak dopamine (DA) release computed as in the experiments of Fig. 2a reveal a distribution that corresponds closely to results in the absence of blockers, albeit with somewhat different spatial coverage (cyan outline) due to infusion variability among animals. Coordinates with respect to bregma noted at bottom right of each coronal slice. **c,**

Mean time courses of NAc dopamine observed in the absence (cyan) and presence (dark blue) of treatment with D1/D2 blockers. Shading denotes SEM of five animals (– blockers) or four animals (+ blockers). **d,** Comparison of mean peak dopamine release amplitudes in absence (cyan) *vs.* presence (dark blue) of D1/D2 inhibitors, over three striatal regions for which data were obtained in both conditions. Error bars denote SEM. All differences not significant with *t*-test $p \geq 0.07$.

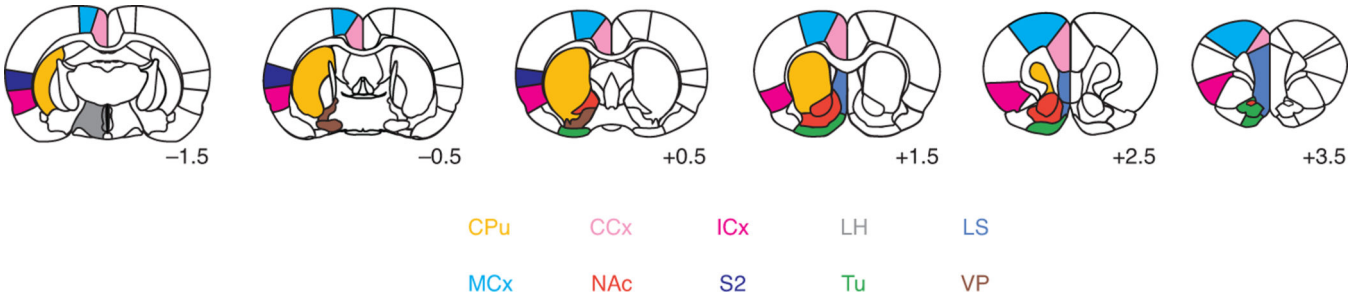

Extended Data Fig. 7 |. Regions of interest used in brain-wide functional connectivity analysis.
Relevant ROIs were defined with respect to standard brain atlases and are shown here color coded by region: caudate-putamen (CPu), cingulate cortex (CCx), insular cortex (ICx), lateral hypothalamus (LH), lateral septal area (LS), motor cortex (MCx), nucleus accumbens (NAc), olfactory tubercle (Tu), secondary somatosensory cortex (S2), ventral pallidum (VP). Coordinates of each slice relative to bregma indicated. Voxel-level definitions of LS, NAc, Tu, and ventromedial CPu are specified in Fig. 2d, and account for experimentally determined anatomical landmarks in ventral striatum, as reflected in the MRI data.

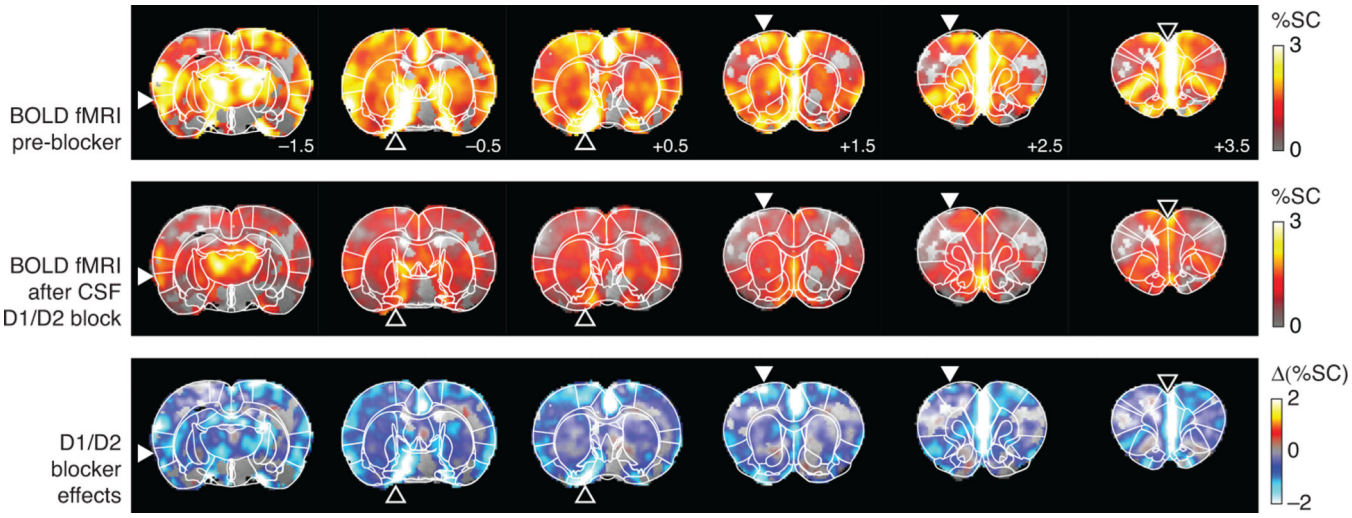

Extended Data Fig. 8 |. Effect of intracerebrospinal fluid D1/D2 inhibitor administration on reward induced brain activation.
Three animals were implanted with a cannula targeting the cerebrospinal fluid (CSF) at the cisterna magna and imaged during rewarding stimulation of LH. Maps show percent signal change (%SC) before (top) and after (middle) infusion of a cocktail containing SCH 23390 and eticloprode, both for voxels with significant activation in the pre-blocker condition ($p \leq 10^{-5}$). The bottom row shows the corresponding difference signal map. Labels in top panel

denote coordinates with respect to bregma. Filled arrowheads note areas of reduced activation in ICx/S2 (–1.5 mm) and MCx (+1.5 and +2.5 mm) observed upon D1/D2 receptor blockade and similar to effects observed with systemic inhibition treatment in Fig. 4a. Open arrowheads denote differences from the systemic treatment results along the midline (+3.5 mm) and in ventral areas (–0.5 and +0.5 mm) that likely received much higher doses of the inhibition cocktail due to proximity to the CSF infusion route.

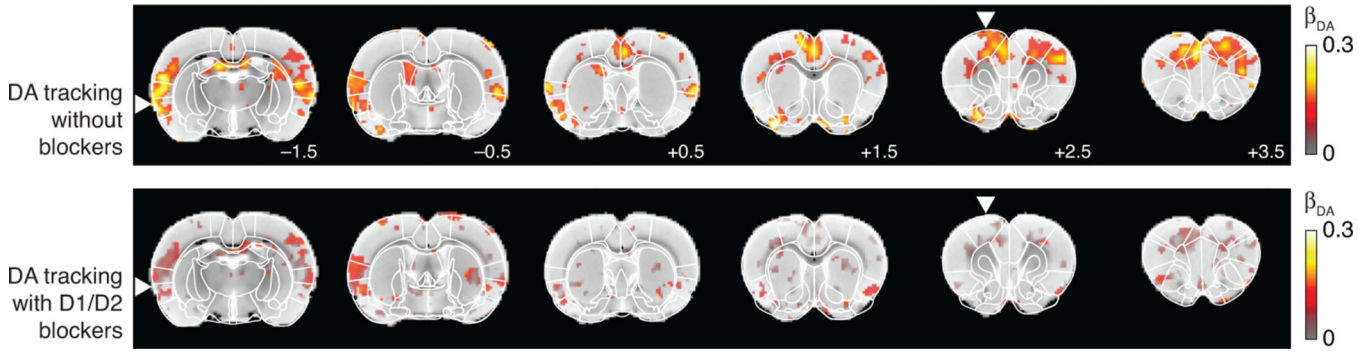

Extended Data Fig. 9 |. Functional connectivity between striatal dopamine and distal BOLD signals before and after D1/D2 receptor blockade.

Regression analysis was used to determine the amplitude of dopamine tracking signals (β_{DA}, *F*-test $p \leq 0.05$) observed throughout the brain in regions distal to 9D7 infusion sites in ventral striatum using methods of Fig. 4c,d. The analysis was performed on two groups of animals, one untreated with SCH 23390 and eticlopride (top, $n = 5$) and one pre-treated with the systemic D1/D2 inhibition cocktail ($n = 4$). In each case, dopamine and BOLD data were obtained from the same animals, and β_{DA} values reflect shared variance of simultaneously acquired temporally varying dopamine and BOLD signals across multiple individuals. Labels in top panel denote coordinates with respect to bregma. Arrowheads highlight areas where D1/D2 blockade substantially reduces tracking behavior in MCx (+2.5 mm) and in ICx and S2 (–1.5 mm).

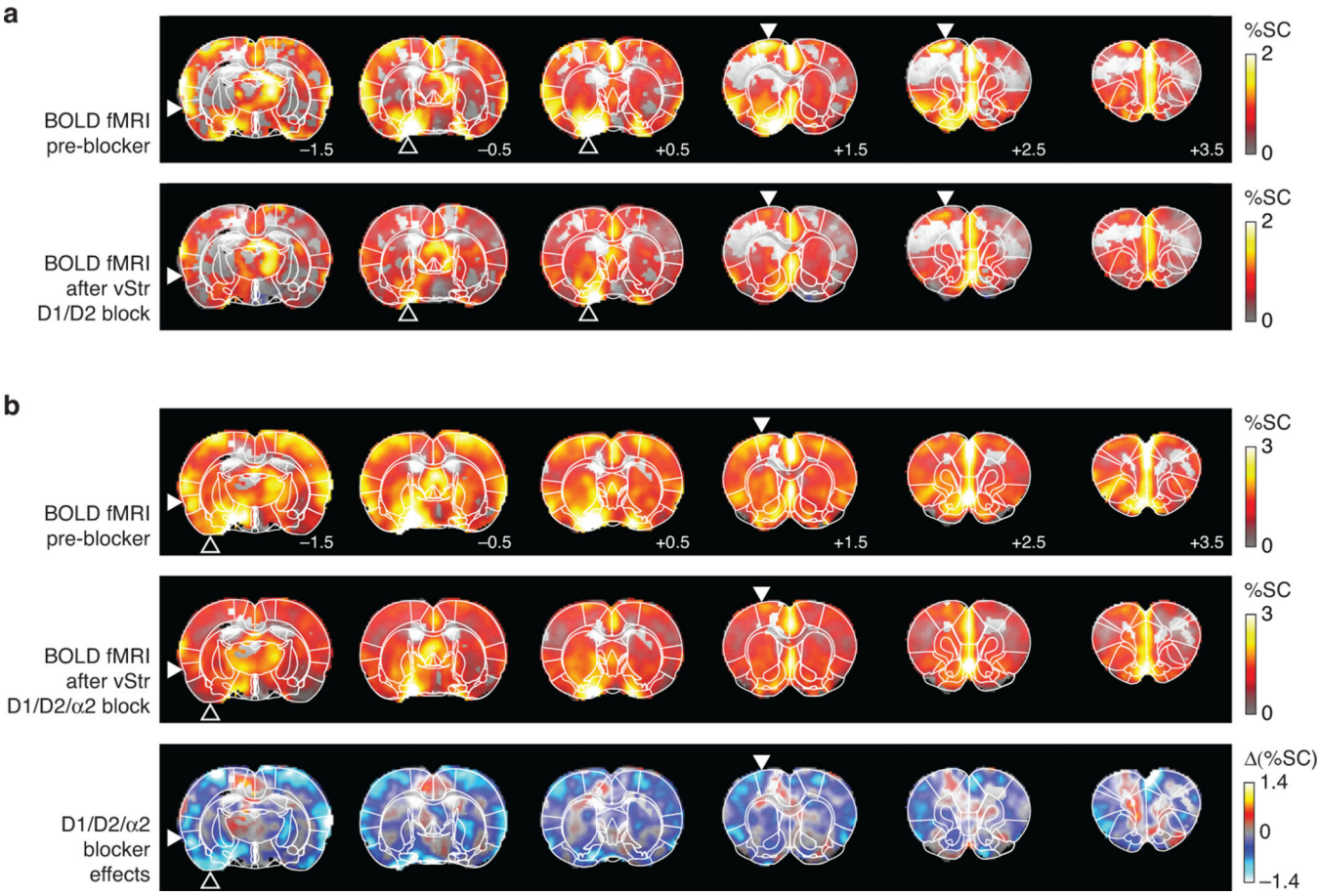

Extended Data Fig. 10 |. Effect of ventral striatal receptor blockade on reward induced brain activation.

a, D1/D2 inhibitors were intracranially infused into five animals implanted with cannulae targeting ventral striatum (vStr) and imaged during rewarding stimulation of LH. Maps show percent signal change (%SC) before (top) and after (middle) administration of a cocktail containing SCH 23390 and eticloprode, both for voxels with significant activation in the pre-blocker condition ($p \leq 10^{-5}$). Corresponding difference map presented as Fig. 4e. Labels in top panel denote coordinates with respect to bregma. Filled arrowheads note areas of highly reduced activation in ICx (–1.5 mm) and MCx (+1.5 and +2.5 mm) observed upon local D1/D2 receptor blockade. Reduced activation in Tu and VP (open arrowheads) likely reflects direct effects of the locally infused dopamine blockers. **b,** A combination of dopamine inhibitors and a norepinephrine inhibitor was intracranially infused into four animals implanted with cannulae targeting ventral striatum (vStr) and imaged during rewarding stimulation of LH. Maps again show percent signal change (%SC) before (top) and after (middle) infusion of a cocktail this time containing SCH 23390, eticloprode, and the α2 receptor antagonist yohimbine, both for voxels with significant activation in the pre-blocker condition ($p \leq 10^{-5}$). The bottom row shows the corresponding difference signal map. Filled arrowheads at bregma –1.5 and +1.5 denote areas in ICx/S2 and MCx where reduction of BOLD signal parallels effects observed with D1/D2 blockade alone (Fig. 4e and

panel **a**). Open arrowhead at bregma –1.5 mm indicates an amygdalar region that may be sensitive to the addition of yohimbine in the treatment mixture.

Supplementary Material

Refer to Web version on PubMed Central for supplementary material.

Acknowledgements

This research was funded by NIH grants R01 DA038642 and U01 NS103470 to AJ. NL was supported by a Stanley Fahn Research Fellowship from the Parkinson's Disease Foundation. The authors thank Taekwan Lee and Lili Cai for initial assistance with the experimental methods. The authors are also grateful to Ann Graybiel, Sabbi Lall, and Ilana Witten for comments on the data and manuscript.

Abbreviations:

BOLD	Blood Oxygen Level-Dependent
CPu	Caudate-Putamen
CCx	Cinculate Cortex
9D7	Cytochrome BM3h-9D7
WT	Cytochrome BM3h-WT
FWHM	Full Width at Half Maximum
fMRI	Functional Magnetic Resonance Imaging
IRF	Impulse Response Function
ICx	Insular Cortex
LH	Lateral Hypothalamus
LS	Lateral Septal Area
MRI	Magnetic Resonance Imaging
MCx	Motor Cortex
NAc	Nucleus Accumbens
Tu	Olfactory Tubercle
ROI	Region of Interest
S2	Secondary Somatosensory Cortex
VP	Ventral Pallidum

References

1. Wise RA Dopamine, learning and motivation. Nat Rev Neurosci 5, 483–494 (2004). [PubMed: 15152198]
2. Berke JD What does dopamine mean? Nat Neurosci 21, 787–793 (2018). [PubMed: 29760524]
3. Bamford NS, Wightman RM & Sulzer D. Dopamine's Effects on Corticostriatal Synapses during Reward-Based Behaviors. Neuron 97, 494–510 (2018). [PubMed: 29420932]
4. Lee T, Cai LX, Lelyveld VS, Hai A. & Jasanoff A. Molecular-level functional magnetic resonance imaging of dopaminergic signaling. Science 344, 533–535 (2014). [PubMed: 24786083]
5. Olds J. & Milner P. Positive reinforcement produced by electrical stimulation of septal area and other regions of rat brain. J Comp Physiol Psychol 47, 419–427 (1954). [PubMed: 13233369]
6. Brustad EM et al. Structure-guided directed evolution of highly selective p450-based magnetic resonance imaging sensors for dopamine and serotonin. J Mol Biol 422, 245–262 (2012). [PubMed: 22659321]
7. Kundu P. et al. Integrated strategy for improving functional connectivity mapping using multiecho fMRI. Proc Natl Acad Sci U S A 110, 16187–16192 (2013). [PubMed: 24038744]
8. Shapiro MG et al. Directed evolution of a magnetic resonance imaging contrast agent for noninvasive imaging of dopamine. Nat Biotechnol 28, 264–270 (2010). [PubMed: 20190737]
9. Krautwald K, Min HK, Lee KH & Angenstein F. Synchronized electrical stimulation of the rat medial forebrain bundle and perforant pathway generates an additive BOLD response in the nucleus accumbens and prefrontal cortex. Neuroimage 77, 14–25 (2013). [PubMed: 23558098]
10. Fiallos AM et al. Reward magnitude tracking by neural populations in ventral striatum. Neuroimage 146, 1003–1015 (2017). [PubMed: 27789262]
11. O'Doherty JP, Dayan P, Friston K, Critchley H. & Dolan RJ Temporal difference models and reward-related learning in the human brain. Neuron 38, 329–337 (2003). [PubMed: 12718865]
12. O'Doherty J. et al. Dissociable roles of ventral and dorsal striatum in instrumental conditioning. Science 304, 452–454 (2004). [PubMed: 15087550]
13. Brocka M. et al. Contributions of dopaminergic and non-dopaminergic neurons to VTA-stimulation induced neurovascular responses in brain reward circuits. Neuroimage 177, 88–97 (2018). [PubMed: 29723641]
14. Logothetis NK The neural basis of the blood-oxygen-level-dependent functional magnetic resonance imaging signal. Philos Trans R Soc Lond B Biol Sci 357, 1003–1037 (2002). [PubMed: 12217171]
15. Mandeville JB et al. A receptor-based model for dopamine-induced fMRI signal. Neuroimage 75, 46–57 (2013). [PubMed: 23466936]
16. Boja JW et al. High-affinity binding of [125I]RTI-55 to dopamine and serotonin transporters in rat brain. Synapse 12, 27–36 (1992). [PubMed: 1411961]
17. Freed C. et al. Dopamine transporter immunoreactivity in rat brain. J Comp Neurol 359, 340–349 (1995). [PubMed: 7499533]
18. Kapogiannis D, Campion P, Grafman J. & Wassermann EM Reward-related activity in the human motor cortex. Eur J Neurosci 27, 1836–1842 (2008). [PubMed: 18371077]
19. Naqvi NH & Bechara A. The hidden island of addiction: the insula. Trends Neurosci 32, 56–67 (2009). [PubMed: 18986715]
20. Marsh BT, Tarigoppula VS, Chen C & Francis JT Toward an autonomous brain machine interface: integrating sensorimotor reward modulation and reinforcement learning. J Neurosci 35, 7374–7387 (2015). [PubMed: 25972167]
21. Arsenault JT, Nelissen K, Jarraya B. & Vanduffel W. Dopaminergic reward signals selectively decrease fMRI activity in primate visual cortex. Neuron 77, 1174–1186 (2013). [PubMed: 23522051]
22. Stuber GD & Wise RA Lateral hypothalamic circuits for feeding and reward. Nat Neurosci 19, 198–205 (2016). [PubMed: 26814589]
23. Lee HJ et al. Activation of Direct and Indirect Pathway Medium Spiny Neurons Drives Distinct Brain-wide Responses. Neuron 91, 412–424 (2016). [PubMed: 27373834]

24. Tritsch NX & Sabatini BL Dopaminergic modulation of synaptic transmission in cortex and striatum. Neuron 76, 33–50 (2012). [PubMed: 23040805]

25. Ferenczi EA et al. Prefrontal cortical regulation of brainwide circuit dynamics and reward-related behavior. Science 351, aac9698 (2016).

26. Decot HK et al. Coordination of Brain-Wide Activity Dynamics by Dopaminergic Neurons. Neuropsychopharmacology 42, 615–627 (2017). [PubMed: 27515791]

27. Nakano T, Doi T, Yoshimoto J. & Doya K. A kinetic model of dopamine- and calcium-dependent striatal synaptic plasticity. PLoS Comput Biol 6, e1000670 (2010).

28. Gerfen CR & Surmeier DJ Modulation of striatal projection systems by dopamine. Annu Rev Neurosci 34, 441–466 (2011). [PubMed: 21469956]

29. Castro LR et al. Striatal neurones have a specific ability to respond to phasic dopamine release. J Physiol 591, 3197–3214 (2013). [PubMed: 23551948]

30. Klein-Flugge MC, Hunt LT, Bach DR, Dolan RJ & Behrens TE Dissociable reward and timing signals in human midbrain and ventral striatum. Neuron 72, 654–664 (2011). [PubMed: 22099466]

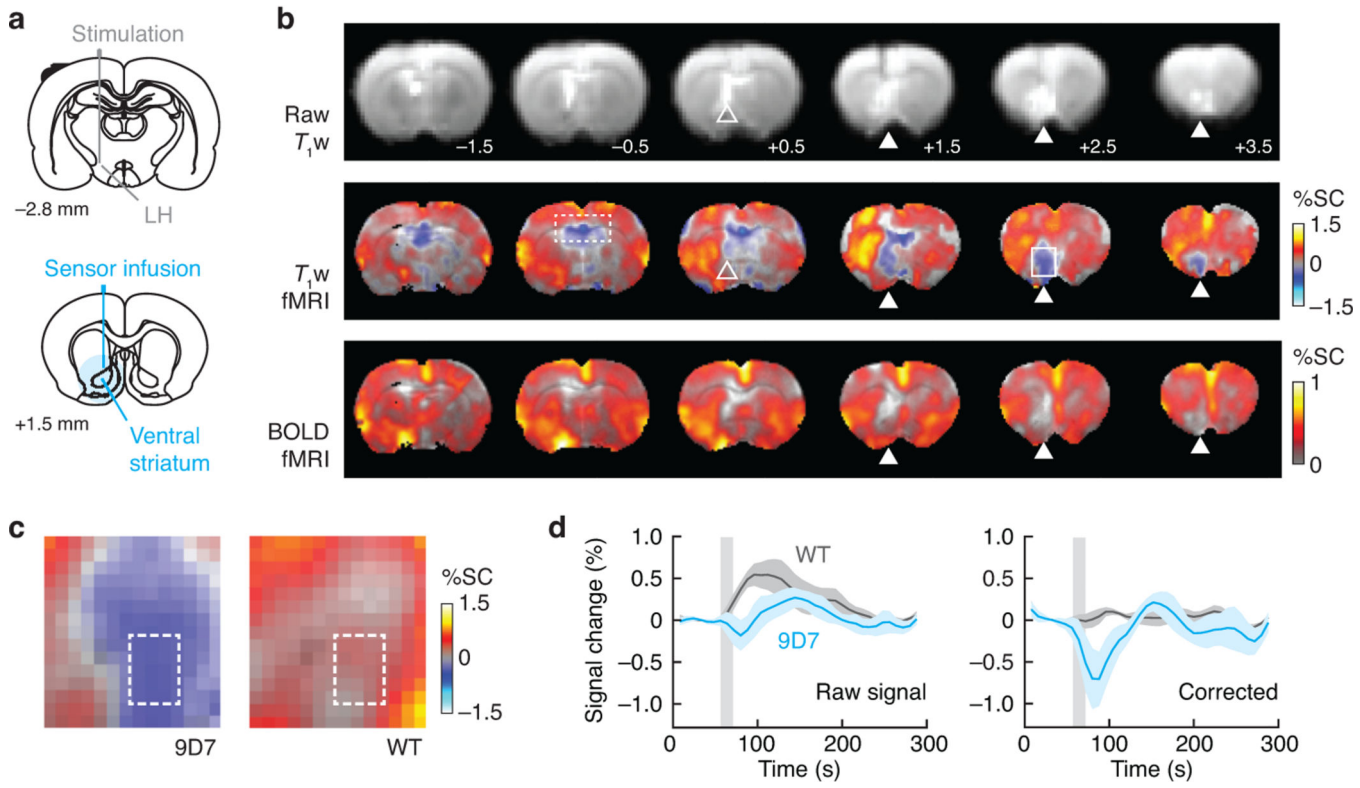

Figure 1 |. Functional and molecular imaging of responses to rewarding stimulation.

a, Stimulation and contrast agent infusion sites used in this study, diagrammed on coronal rat brain sections (bregma coordinates indicated). Stimulation electrodes (gray) are targeted to lateral hypothalamus (LH) and ipsilateral (cyan) are targeted to ipsilateral ventral striatum. **b,** Six 1 mm slices were imaged using a multiecho pulse sequence that permits simultaneous T_1-weighted (T_1w) and BOLD fMRI data collection: (top) raw T_1w signal (bregma coordinates shown); (middle) T_1w fMRI signal change evoked by LH stimulation; (bottom) BOLD fMRI signal estimated from multiecho data. Areas of peak contrast agent infusion (filled arrowheads) correspond to negative T_1w fMRI signal change and suppression of hemodynamic contrast (Extended Data Fig. 2). Negative T_1w fMRI signals do not colocalize with raw T_1w enhancement in lateral ventricles (open arrowheads), but do occur near the corpus callosum (dashed box) in both 9D7-injected and uninjected animals (Extended Data Fig. 2a). **c,** Close up of solid boxed region in **b**, comparing negative signal change mediated by the 9D7 dopamine sensor to the neutral effect of the WT control protein, which merely suppresses regional T_1w hemodynamic signal changes. **d,** Mean time courses of 9D7-mediated dopamine-dependent T_1w fMRI signal changes (cyan) and control dopamine-independent WT signal changes (gray) evoked by LH stimulation (vertical gray bar), evaluated over boxed regions in **c**, before (left) and after (right) correction for residual hemodynamic responses. Shading depicts SEM for $n = 5$.

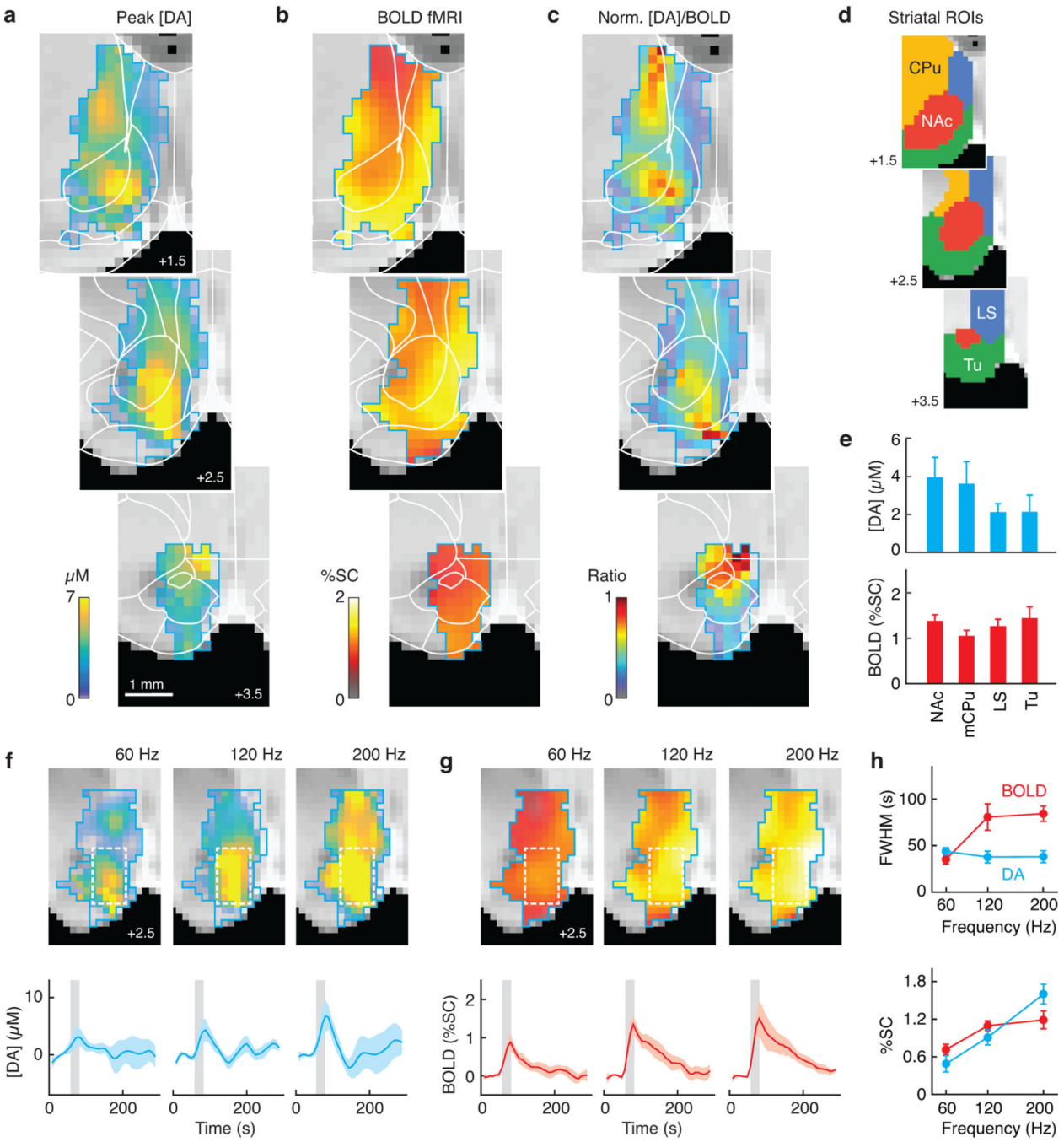

Figure 2 |. Dissociable profiles of reward-evoked striatal dopamine release and BOLD activation.

a, Peak rewarding stimulus-evoked dopamine release amplitudes (color) averaged over sensor infused regions from five animals (cyan outline). Anatomical MRI shown as underlay and atlas regions indicated by white outline. **b,** Stimulus-evoked BOLD fMRI signal amplitudes in the contrast agent-infused region of **a**. **c,** Normalized ratio of profiles in **a** and **b**, indicating lack of spatial correspondence between dopamine and BOLD amplitudes. **d,** Definition of striatal subregions in medial caudate-putamen (CPu), nucleus accumbens (NAc), lateral septal area (LS), and olfactory tubercle (Tu). **e,** ROI-averaged dopamine

amplitudes (cyan) and BOLD signal changes (red) in each striatal subregion. Error bars indicate SEM over five animals. **f,** Dopamine release amplitudes maps (top) as a function of rewarding stimulus frequency as indicated, with corresponding time courses for dashed region shown (bottom). Shading indicates SEM ($n = 5$). **g,** BOLD profiles shown as a function of stimulus frequency above, with corresponding time courses below. **h,** Frequency-dependence of full width at half maximum (FWHM, top) and percent signal change (%SC, bottom) for dopamine (DA, cyan) and BOLD (red) responses to rewarding stimulation. SEMs indicated ($n = 5$).

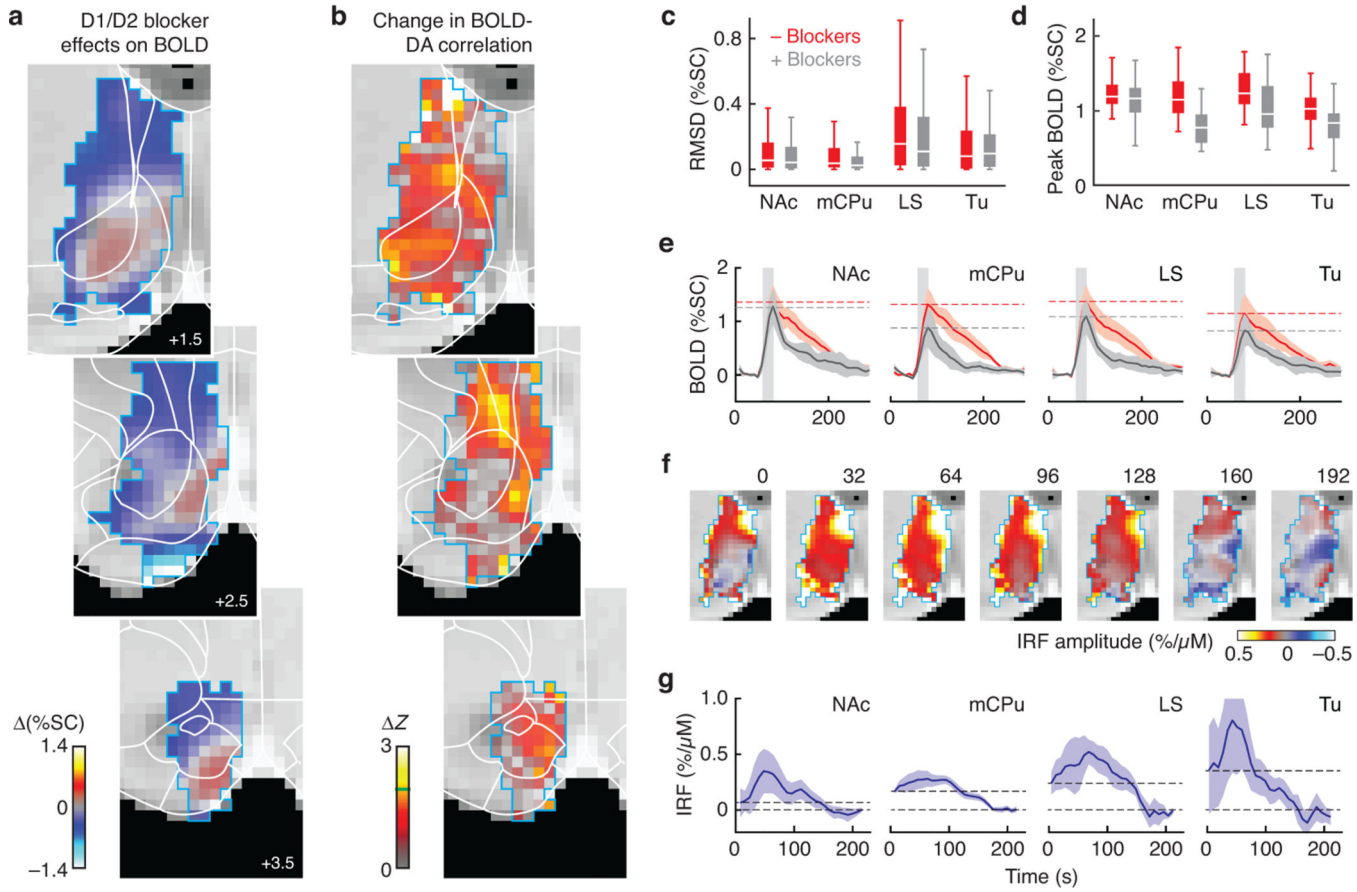

Figure 3 |. Dopamine-dependent modulation of striatal fMRI signals.

a, The change in BOLD signal amplitude, Δ(%SC), in response to rewarding stimulation upon addition of D1 and D2 dopamine receptor inhibitors in the contrast agent-infused region of Fig. 2 (cyan outline). **b,** Change in *Z*-value (Δ*Z*) for the correlation between BOLD and dopamine signals upon addition of D1/D2 blockers. Increased correlation is statistically significant at an individual voxel level for $\Delta Z \geq 2.0$ (green line in color scale). **c,** Root mean squared deviation (RMSD) from direct proportionality between dopamine and BOLD response magnitudes across voxels in striatal subregions, before (red) and after (gray) D1/D2 inhibitor treatment. Boxes denote median (center line), first and third quartiles (box edges), and full range of values (whiskers) in each ROI (outliers not shown). **d,** Peak fMRI signal change in response to rewarding stimulation in the absence (red) and presence (gray) of dopamine receptor blockers. Boxes defined as in **c**. **e,** Mean BOLD response to rewarding stimulation (vertical gray bar) in each striatal subregion, before (red) and after (gray) dopamine inhibitor treatment. Horizontal dashed lines denote peak amplitudes. Shading represents SEM for $n = 5$ animals. **f,** Spatially-resolved impulse response function (IRF) describing the effect of dopamine on the BOLD fMRI signal at multiple time points, labeled in seconds. **g,** Mean dopamine-dependent IRFs measured from individual striatal subregions. Shading denotes SEMs ($n = 5$). Dashed lines indicate the instantaneous effect of dopamine on BOLD amplitudes (IRF at time $t = 0$ s).

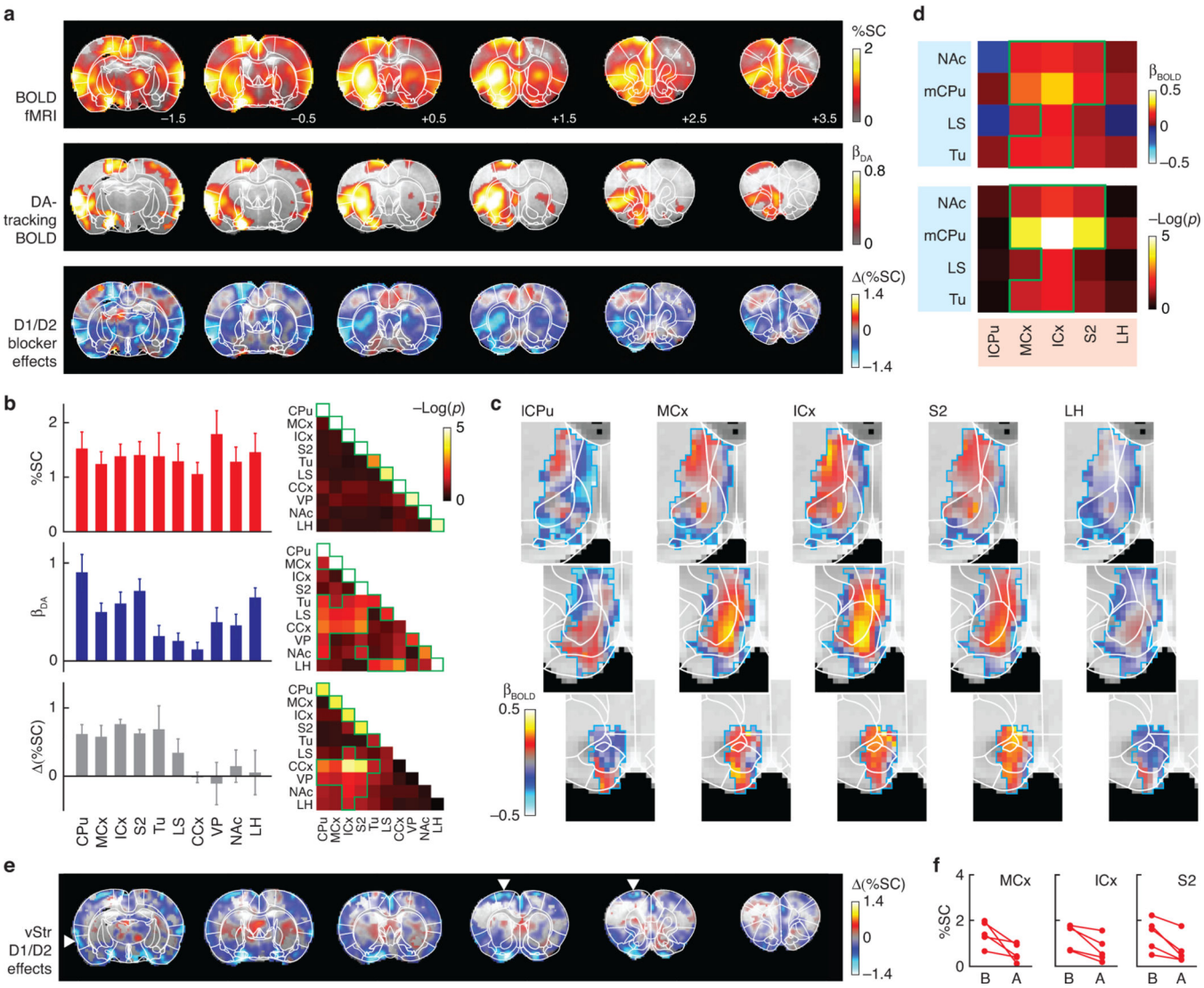

Figure 4 |. Brain-wide consequences of reward-evoked striatal dopamine release.

a, Comparison of brain-wide BOLD fMRI responses to rewarding LH stimulation (%SC, top), dopamine timecourse-tracking components computed by linear regression (β_{DA}, middle), and modulation of fMRI amplitudes by systemic D1/D2 blocker treatment [Δ(%SC), bottom]. Atlas shown as overlay and bregma coordinates noted in top panels. Color overlays masked to display voxels with significant responses to stimulation ($p \leq 10^{-5}$, top and bottom rows) or tracking behavior ($p \leq 0.05$, middle row). **b,** Mean BOLD amplitudes (top), dopamine tracking components (middle), and D1/D2 blocker-dependent fMRI modulations (bottom) averaged over CPu, motor cortex (MCx), insular cortex (ICx), secondary somatosensory cortex (S2), Tu, LS, cingulate cortex (CCx), ventral pallidum (VP), NAc, and LH. All shown with SEM for $n = 5$. Matrices at right specify *t*-test *p*-values for significance of individual ROI averages (diagonal) and differences between ROIs (off-diagonal); values with $p \leq 0.05$ outlined in green. **c,** Correspondence between simultaneously-acquired striatal dopamine and distal fMRI responses from five regions, computed by linear regression of the dopamine signal to yield maps of BOLD-tracking

amplitudes (β_{BOLD}). **d,** ROI averages of data in **c**, presented as mean β_{BOLD} values (top) with corresponding *t*-test *p*-values for statistical significance (bottom) between striatal subregions (vertical axis) and distal BOLD signals (horizontal axis). Values with $p \leq 0.05$ outlined in green. **e,** Modulation of fMRI signals produced by infusion of D1/D2 blockers into ventral striatum. Arrowheads highlight key areas of similarity with the results of panel **b**. **f,** Consistent long-range effects of striatal dopamine inhibition are observed in MCx, ICx, and S2; all differences before (B) *vs.* after (A) treatment are significant with paired *t*-test $p \leq 0.05$, $n = 5$.